Author Contributions:

Conceptualization: Ilya Usoskin, Gennady A. Kovaltsov
Data curation: Sergey Koldobskiy
Formal analysis: Sergey Koldobskiy
Methodology: Sergey Koldobskiy, Ilya Usoskin, Gennady A. Kovaltsov
Supervision: Ilya Usoskin
Validation: Gennady A. Kovaltsov
Writing – original draft: Sergey Koldobskiy, Ilya Usoskin
Writing – review & editing: Sergey Koldobskiy, Ilya Usoskin, Gennady A. Kovaltsov

Effective Energy of Cosmogenic Isotope (^{10}Be, ^{14}C and ^{36}Cl) Production by Solar Energetic Particles and Galactic Cosmic Rays

Sergey Koldobskiy[1,2] [iD], **Ilya Usoskin[1,3]** [iD], **and Gennady A. Kovaltsov[1,4]**

[1]University of Oulu, Oulu, Finland, [2]National Research Nuclear University MEPhI, Moscow, Russia, [3]St.Petersburg State University, St. Petersburg, Russia, [4]Ioffe Physical-Technical Institute RAS, St. Petersburg, Russia

Abstract Cosmogenic isotopes ^{14}C, ^{10}Be and ^{36}Cl measured in datable natural archives provide the only known quantitative proxy for cosmic-ray (CR) and solar-activity variability before the era of direct measurements. Studies of relations between the measured isotope concentrations and CR variability require complicated modeling including the isotope production and transport in the terrestrial system. Here we propose a rough "effective energy" method to make quick estimates of the CR variability directly from the cosmogenic data using an approximate linear scaling between the measured isotope concentrations and the energy-integrated flux of CR above the effective energy. The method is based on the thoroughly computed effective yield function presented here. A simple way to account for the variable geomagnetic field is also provided. The method was developed for both solar energetic particles (SEPs) and galactic cosmic ray (GCR) variability and is shown to provide a robust result within 20% and 1% accuracy, respectively, without an assumption of the specific spectral shape. Applications of the effective-energy method to the known extreme SEP events and the secular GCR variability are discussed. The new method provides a simple and quick tool to assess the CR variability in the past. On the other hand, it does not supersede the full detailed modeling required for precise results.

1. Introduction

Energetic cosmic rays bombard the Earth's atmosphere and cause nucleonic-muon-electromagnetic cascades, where, in particular, different radioactive isotopes can be produced. Since these isotopes are not naturally present in the terrestrial environment, and their only (or dominant) source on Earth is the production by cosmic rays, they are called cosmogenic and form a quantitative proxy for the cosmic-ray (and thus solar and geomagnetic) variability in the past, before the instrumental era (e.g., Beer et al., 2012; Wu et al., 2018). In addition to galactic cosmic rays (GCRs) which always bombard the Earth's atmosphere, sporadic events with enhanced fluxes of solar energetic particles (SEPs) occur as caused by solar eruptive phenomena such as flares and/or coronal mass ejections (e.g., Desai & Giacalone, 2016; Vainio et al., 2009). When SEPs are accelerated to sufficiently high energies (above several hundred MeV), they can initiate nucleonic-muon-electromagnetic cascades in the atmosphere that can be detected on the ground. Such SEP events are called ground-level enhancements (GLEs) – see the definition in Poluianov et al. (2017). Usually, fluxes of SEPs are insufficient to produce a detectable amount of cosmogenic isotopes (Usoskin et al., 2020), but rarely, SEP events can be extremely strong to be clearly identified in the cosmogenic-isotope natural archives (e.g., Miyake et al., 2020). A detailed analysis of the measured cosmogenic-isotope data with a task to reconstruct parameters of solar variability or SEP energy spectra requires sophisticated modeling of the isotope production, transport and deposition (e.g., Büntgen et al., 2018; Jull et al., 2014; Sukhodolov et al., 2017).

Most important cosmogenic isotopes are (e.g., Beer et al., 2012): ^{14}C known as radiocarbon, which is produced as a result of ^{14}N(n, p)^{14}C reactions, takes a part in the global carbon cycle, and is measured in samples of living or dead trees; ^{10}Be, which is produced as a result of spallation of atmospheric oxygen and nitrogen, is partly mixed in the atmosphere and deposited in polar regions where it is measured in ice cores; ^{36}Cl is produced by spallation of argon and takes part in the chlorine cycle and is also measured in polar ice cores. This is somewhat similar to a ground-based neutron monitor (NM), which measures the nucleonic component of local cosmic-ray-induced atmospheric cascades (Simpson, 2000), but is different in that it includes also transport of the isotope in the terrestrial system and its deposition to an archive (Beer, 2000). Accordingly, the measured cosmogenic-isotope

concentrations correspond not to the local cosmic-ray-induced cascades but to a weighted flux of cosmic rays distributed over the globe. Generally, the production and transport of cosmogenic isotopes in the terrestrial atmosphere can be considered as an energy-integrating distributed cosmic-ray detector, which does not directly measure the energy spectrum but rather the integral response. The response is defined by the yield function of the detector (see details in Section 2). The ideal integral detector should have a step-like yield function characterized by a threshold energy E_{th} so that the detector's efficiency is zero and unity for energies below and above E_{th}, respectively. Such a detector could directly measure the integral flux of cosmic rays with energy above the threshold. The realistic yield function of cosmogenic isotope production is not step-like but grows with the particle's energy (Poluianov et al., 2016). However, in some cases, the so-called effective energy E_{eff} exists that reduces the real detector to the ideal one with E_{eff} being the threshold energy, with no or little dependence on the exact spectral shape.

The concept of effective energy was introduced to study GCR variability (Alanko et al., 2003; Asvestari, Gil, et al., 2017) and SEPs (Koldobskiy, Kovaltsov, et al., 2019) using data from the NM network as well as for cosmogenic isotope production in lunar rocks (Poluianov et al., 2018). The effective-energy concept was applied by Kovaltsov et al. (2014) to the production of cosmogenic isotopes ^{14}C and ^{10}Be in terrestrial archives by SEP events. In this paper, we further develop the concept of the effective energy for cosmogenic isotopes using updated yield functions (Poluianov et al., 2016) and revisited energy spectra of SEP/GLE events (Koldobskiy et al., 2021). We also consider GCR directly measured by AMS-02 (Aguilar et al., 2018a).

2. Modeling

The concept of effective energy E_{eff} or rigidity is based on an assumption (and its validation) that the energy-integrated flux (in the number of particles per [cm² sr s]) of cosmic rays with energy above it $J(>E_{eff})$ is roughly proportional to the measured quantity Q:

$$J(>E_{eff}) = \mathcal{K}_{eff} \cdot Q, \tag{1}$$

Since the intensity of SEP/GLE events is usually characterized by the energy-integrated omnidirectional fluence $F(>E)$ (in units of particles per cm²), this equation for SEP/GLE events is

$$F(>E_{eff}) = \mathcal{K}_{eff} \cdot Q, \tag{2}$$

For cosmogenic isotopes, Q can be the depositional flux (in the framework of a specific transport model) or the production rate and can be represented as (see the full formalism in Section 3 of Asvestari, Gil, et al., 2017):

$$Q = \sum_i \int_0^\infty A_i \cdot J_i(E) \cdot Y_{eff,i}(E, M) \cdot dE, \tag{3}$$

where the summation is over different species of cosmic-ray particles, $J_i(E)$ is the differential energy spectrum of particles of the ith type with the atomic mass A_i, $Y_{eff,i}(E, M)$ is the isotope's effective yield function for nucleons, which depends on the geomagnetic field characterized by the virtual axial dipole moment (VADM – Korte & Constable, 2005) M and transport of the isotope in the atmosphere. The differential energy spectrum is related to the omnidirectional integrated flux as

$$J(E) = \frac{1}{4\pi} \cdot \frac{dF(>E)}{dE}. \tag{4}$$

All the computations here were made for the reference present-day VADM of $M_0 = 7.75 \cdot 10^{22}$ A m² (Thébault et al., 2015). Corrections for other VADM values for both SEP and GCR are described in Section 3.3.

Here we computed the effective yield functions for the three isotopes applying the formalism described by Asvestari, Gil, et al. (2017). We used specific yield functions provided in Poluianov et al. (2016). Global production was considered for ^{14}C, while transport/deposition of ^{10}Be and ^{36}Cl in polar ice was modeled using parameterization by Heikkilä et al. (2009) and Heikkilä et al. (2013). The computed effective yield functions for primary cosmic ray protons are shown in Figure 1 and tabulated in the Supporting Information S1.
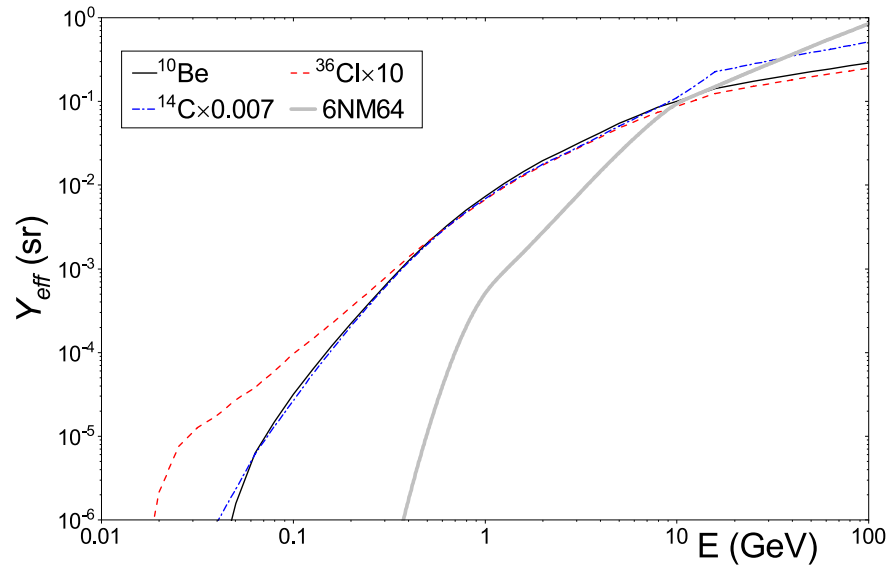
Figure 1. Effective yield functions of the cosmogenic isotope production/deposition for the three isotopes, considered here, viz. ^{10}Be and ^{36}Cl in polar ice as well as global ^{14}C. The yield function is shown for primary cosmic-rays protons. They were computed for the modern geomagnetic field strength ($M = 7.75 \cdot 10^{22}$ A m^2) using the yield functions from Poluianov et al. (2016) and assuming global production for ^{14}C and transport/deposition model by Heikkilä et al. (2013) for ^{10}Be and ^{36}Cl. The values are tabulated in the Supporting Information S1. The curves were scaled, as indicated in the legend, for better visibility. For comparison, the yield function (in sr m^2) of a polar sea-level 6NM64 (Mishev et al., 2020) is also shown.

3. Effective Energy for Solar Energetic Particles

3.1. Differential Response Function

The product of the energy spectrum and the effective yield function, viz. the integrand of Equation 3, is called the differential response function $D = J \cdot Y_{eff}$ and quantifies the sensitivity of the isotope production/deposition to the energy of primary cosmic-ray particles. As an illustration, Figure 2b shows the differential response functions for the GLE event #5 of 23 February 1956 which was the strongest directly observed event with the hardest known spectrum. One can see that ^{14}C and ^{10}Be have very similar responses with the highest sensitivity to SEPs of a few hundred MeV; ^{36}Cl is sensitive to lower-energy SEPs (several tens of MeV); while NM is sensitive to SEPs with the energy of around one GeV. Basing on the significant difference between the peaks for ^{36}Cl and ^{10}Be, a rough assessment method of the extreme SPE spectral characteristics was proposed by Webber et al. (2007) and applied for recent events (Mekhaldi et al., 2015; O'Hare et al., 2019). Figure 2c depicts the cumulative relative contributions to the production/deposition Q. Crossings of the cumulative curves with the horizontal line denote the median energies of the isotope production. The median energy varies significantly (not shown) between the analyzed GLE events, especially for ^{36}Cl, and thus cannot be used as effective energy of cosmogenic isotope production.

3.2. Effective Energy

In this Section, we determine the effective energy of cosmogenic isotope production by SEPs as defined by Equation 2.

Here we considered all GLE events with reliably defined spectra, viz. 58 events with the reconstructed proton energy spectra (see Table 2 in Koldobskiy et al., 2021). Contribution of helium and heavier species into the cosmogenic-isotope production is small (less than 5%) for SEPs (Mekhaldi et al., 2015, 2021). The time resolution of the cosmogenic data is typically annual, and a sophisticated analysis can lead to, at best, seasonal accuracy of the isotope production (e.g., Büntgen et al., 2018; Sukhodolov et al., 2017; Uusitalo et al., 2018). Accordingly, individual SEP events cannot be distinguished in the cosmogenic-isotope data from a series of consecutive events originating from the same solar active region, as for example, took place in 1989. Therefore, we have combined SEP events into annual SEP fluences by summing up fluences of individual events over a calendar year. Thirty
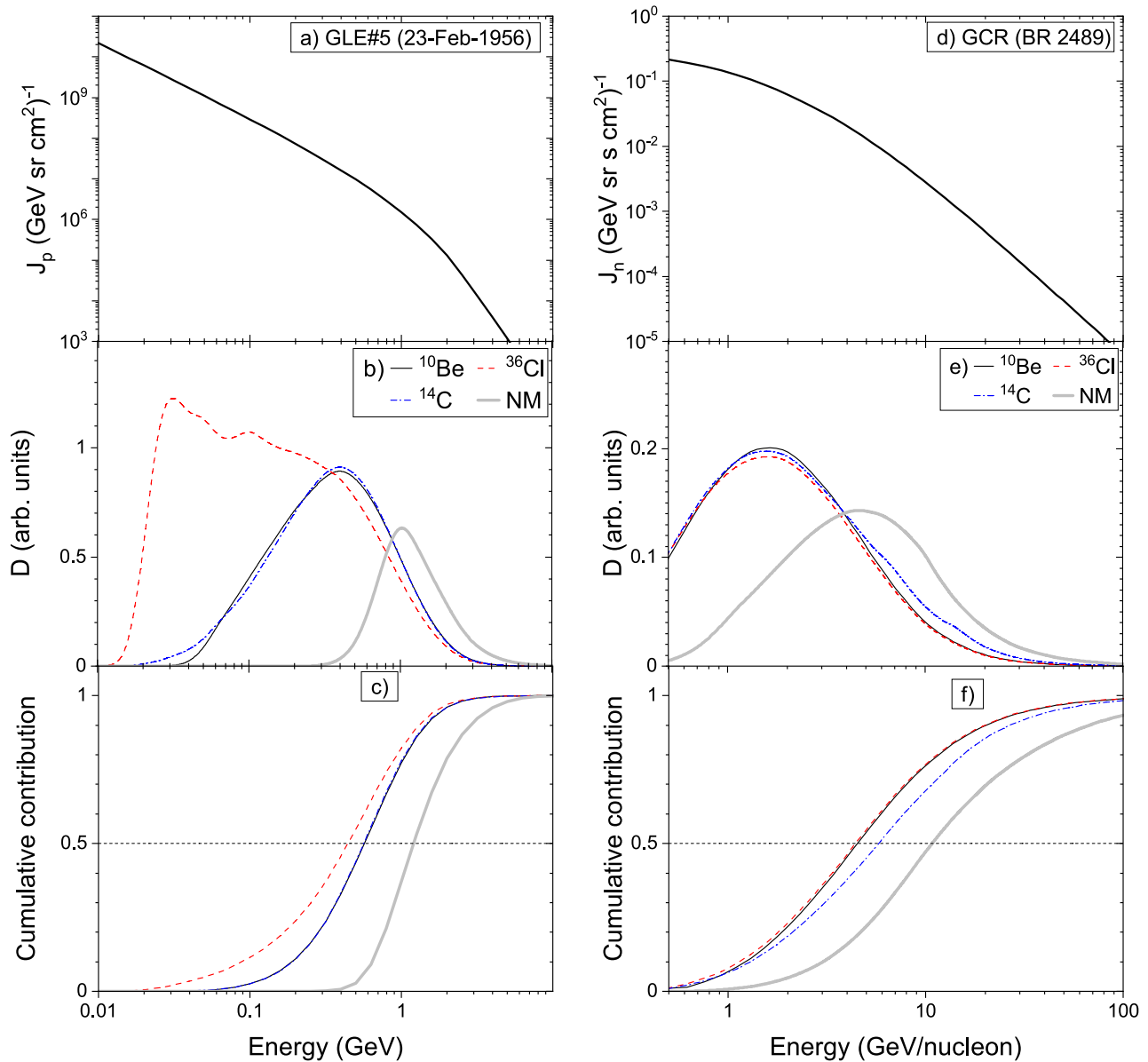
Figure 2. Panel (a): differential energy spectrum of GLE#5 (Koldobskiy et al., 2021). Panel (b): differential response functions for the three isotopes and a polar sea-level NM for GLE#5. Panel (c): cumulative relative contribution $\int_0^E D(E')/Q \cdot dE'$ for the three isotopes and NM for GLE#5. The dotted horizontal line denotes the 0.5 contribution, viz. the median. Panels (d–f) are similar to panels (a–c) but for galactic cosmic-ray nucleons for BR 2489 (10 January 2016 through 05 February 2016).

yearly SEP fluences were made as shown in Table 1. We used these annual fluences as an input for the production model (Equation 3).

For all annual-fluence spectra, we computed, using Equation 3, the corresponding productions Q of each isotope as shown in Table 1. One can see that the annual SEP-related production varies by up to three orders of magnitude between different years. Next, we calculated the scaling factor as a function of energy following Equation 2, viz. $\mathcal{K}(E) = F(>E)/Q$. Figures 3a–3c show the relation between $\mathcal{K}$ and E for different cosmogenic isotopes. The relations for individual annual fluences are shown by gray curves. One can see that, despite the huge difference in the annual isotope production rates, all the gray curves cross at nearly the same location, making a "bow-tie" plot (e.g., Raukunen et al., 2020), implying the existence of the effective energy so that Equation 2 is valid irrespectively of the exact spectrum of SEPs.

Table 1
Annual Production/Deposition of Cosmogenic Isotopes by GLE Events

Year[a]	GLE #s[b]	Q_{10Be}[c]	Q_{36Cl}[d]	Q_{14C}[e]
1956	5	$2.34 \cdot 10^4$	$2.66 \cdot 10^3$	$3.13 \cdot 10^6$
1960	8, 10–12	$9.11 \cdot 10^3$	$1.73 \cdot 10^3$	$1.22 \cdot 10^6$
1961	13	$8.53 \cdot 10^2$	$1.80 \cdot 10^2$	$1.14 \cdot 10^5$
1967	16	$6.80 \cdot 10^2$	$9.69 \cdot 10^1$	$9.12 \cdot 10^4$
1968	18, 19	$2.12 \cdot 10^2$	$8.48 \cdot 10^1$	$2.91 \cdot 10^4$
1969	20, 21	$3.99 \cdot 10^2$	$5.49 \cdot 10^1$	$5.33 \cdot 10^4$
1971	22, 23	$1.01 \cdot 10^3$	$2.61 \cdot 10^2$	$1.38 \cdot 10^5$
1972	24, 25	$6.15 \cdot 10^3$	$2.31 \cdot 10^3$	$8.29 \cdot 10^5$
1973	26	$3.13 \cdot 10^1$	$5.43 \cdot 10^0$	$4.17 \cdot 10^3$
1976	27	$6.03 \cdot 10^1$	$1.32 \cdot 10^1$	$8.11 \cdot 10^3$
1977	28–30	$4.30 \cdot 10^2$	$8.25 \cdot 10^1$	$5.80 \cdot 10^4$
1978	31, 32	$2.71 \cdot 10^2$	$7.87 \cdot 10^1$	$3.70 \cdot 10^4$
1979	33	$3.70 \cdot 10^1$	$2.34 \cdot 10^1$	$5.32 \cdot 10^3$
1981	35, 36	$3.15 \cdot 10^2$	$1.13 \cdot 10^2$	$4.37 \cdot 10^4$
1982	37, 38	$2.27 \cdot 10^2$	$5.46 \cdot 10^1$	$3.09 \cdot 10^4$
1984	39	$6.81 \cdot 10^1$	$1.29 \cdot 10^1$	$9.15 \cdot 10^3$
1989	40–46	$1.53 \cdot 10^4$	$2.45 \cdot 10^3$	$2.03 \cdot 10^6$
1990	47–50	$8.79 \cdot 10^2$	$1.21 \cdot 10^2$	$1.17 \cdot 10^5$
1991	51, 52	$7.03 \cdot 10^2$	$1.34 \cdot 10^2$	$9.35 \cdot 10^4$
1992	53	$7.49 \cdot 10^1$	$1.50 \cdot 10^1$	$1.00 \cdot 10^4$
1997	55	$5.47 \cdot 10^2$	$9.56 \cdot 10^1$	$7.29 \cdot 10^4$
1998	56, 58	$9.20 \cdot 10^1$	$1.79 \cdot 10^1$	$1.23 \cdot 10^4$
2000	59	$2.81 \cdot 10^3$	$8.39 \cdot 10^2$	$3.79 \cdot 10^5$
2001	60–63	$2.13 \cdot 10^3$	$4.96 \cdot 10^2$	$2.88 \cdot 10^5$
2002	64	$1.15 \cdot 10^2$	$2.42 \cdot 10^1$	$1.54 \cdot 10^4$
2003	65–67	$2.15 \cdot 10^3$	$1.14 \cdot 10^3$	$3.04 \cdot 10^5$
2005	69	$2.94 \cdot 10^3$	$4.20 \cdot 10^2$	$3.94 \cdot 10^5$
2006	70	$5.63 \cdot 10^2$	$1.05 \cdot 10^2$	$7.51 \cdot 10^4$
2012	71	$8.73 \cdot 10^1$	$1.62 \cdot 10^1$	$1.17 \cdot 10^4$
2017	72	$6.55 \cdot 10^2$	$1.68 \cdot 10^2$	$8.72 \cdot 10^4$

Note. GLE, ground-level enhancement.

[a]Years with GLE events. [b]The events (see the numbering at https://gle.oulu.fi) included into the annual fluences. [c]Deposition of ^{10}Be (polar ice) (in atoms/cm^2). [d]Deposition of ^{36}Cl (polar ice) (in atoms/cm^2). [e]Global production of ^{14}C, (in atoms/cm^2).

The effective energy E_{eff} is defined as the energy where the relative dispersion of individual curves in Figure 3 is minimal. The relative dispersion was quantified as follows. Vertical slices of the $\mathcal{K}$-vs-E plots (Figure 3) were taken for different values of E. For each such slice, the distribution of $\mathcal{K}(E)$ values was constructed, and the mean $<\mathcal{K}>$ and the dispersion $\sigma_{\mathcal{K}}$ were computed. Their ratio, wiz. the relative dispersion of the scaling factor $\sigma_{\mathcal{K}}/<\mathcal{K}>$ was used as the merit function so that we defined the effective energy E_{eff} as the value of energy E which minimizes the relative dispersion as shown in Figure 4.

The best-fit scaling factor $\mathcal{K}_{eff}$ is defined as the mean value over all individual curves, corresponding to E_{eff}, viz. $<\mathcal{K}(E_{eff})>$, and its 68% uncertainties are taken as $\sigma_{\mathcal{K}}(E_{eff})$. The uncertainties of the E_{eff} are defined as the 68% range of the energies at the best-fit $\mathcal{K}_{eff}$ for individual curves. The values and 68% confidence intervals of the effective energies and scaling factors are shown by the red crosses in Figures 3a–3c and given in the central block of Table 2 for the three isotopes studied here.

One can see that the E_{eff} is defined quite accurately, within 11%. The effective energy appears to be 230–240 MeV for ^{14}C and ^{10}Be, in agreement with a previous study by Kovaltsov et al. (2014), but lower (≈ 60 MeV) for ^{36}Cl. The scaling factors are different by up to four orders of magnitude between different isotopes, from 44 for ^{14}C to $\approx 5 \cdot 10^5$ for ^{36}Cl but $\mathcal{K}_{eff}$ is very stable for each individual isotope and is defined with the accuracy of better than 25%.

Quite often, the ratio of $F(>30$ MeV$)/F(>200$ MeV$)$ is considered as an estimate of a measure of the hardness of the SEP spectrum for extreme events (e.g., Asvestari, Willamo, et al., 2017; Cliver et al., 2020; Mekhaldi et al., 2021), where $F(>200$ MeV$)$ is roughly related to the effective energy of ^{14}C production (Kovaltsov et al., 2014), while $F(>30$ MeV$)$ is a typical quantity for SEP fluence based on direct in-situ measurements during the space era (e.g., Shea & Smart, 1990). However, as shown here, the effective energy of ^{36}Cl production/deposition is about 60 MeV, and $F(>30$ MeV$)$ cannot be reliably defined from cosmogenic-isotope data. Accordingly, the $F(>60$ MeV$)/F(>240$ MeV$)$ ratio ought to be used instead.

3.3. Dependence on the Geomagnetic Field

Figure 3 corresponds to the current epoch with the geomagnetic field dipole moment of $M = 7.75 \cdot 10^{22}$ A m^2. However, extreme SEP events detectable in the cosmogenic isotopes occur during different times over millennia (e.g., Miyake et al., 2020), when the geomagnetic shielding can be different. Accordingly, we modeled the isotope production for different values of M ranging from $(6–12) \cdot 10^{22}$ A m^2 as corresponding to the VADM variability during the last 10 millennia of the Holocene (e.g., Korte et al., 2011; Usoskin et al., 2016). The effective energy E_{eff} appears amazingly independent on the geomagnetic field in a wide range of the VADM values: E_{eff} changes within 2% in the full range of the M-values that is much smaller than the 68% confidence intervals for E_{eff} of 8–11% (Table 2). Thus, the effective energy is defined unambiguously and very accurately for SEPs for a broad range of the VADM values. The scaling factor changes more significantly, within ±20%, viz. larger than the error bars, following the corresponding changes in the production. The changes are systematic and can be accurately (within 0.2% in the range of M of $[6–12] \cdot 10^{22}$ A m^2) approximated (see Figure 5a) as:

$$Q(M) = Q_{M_0} \cdot \left(\frac{M_0}{M}\right)^{\gamma}, \qquad (5)$$

Table 2

The Effective Energy E_{eff}, the Scaling Factor $\mathcal{K}_{eff}$, and the Parameter γ of the Relation for the Virtual Axial Dipole Moment (VADM, Equation 5), Calculated Here for the Three Cosmogenic Isotopes, for Solar Energetic Particle (SEP) (Central Block) and for Galactic Cosmic Ray (GCR) (Right-Hand-Side Block)

	SEP			GCR		
Isotope	E_{eff} (MeV)	$\mathcal{K}_{eff}$	γ	E_{eff} (GeV)	$\mathcal{K}_{eff}$ (sr^{-1})	γ
^{14}C	234 ± 18	44 ± 6	0.537	2.48 ± 0.02	$(6.3 \pm 0.03) \cdot 10^{-2}$	0.546
^{10}Be	236 ± 16	$(6.0 \pm 0.8) \cdot 10^{3}$	0.507	2.0 ± 0.02	12.9 ± 0.05	0.364
^{36}Cl	60 ± 7	$(4.7 \pm 0.9) \cdot 10^{5}$	0.513	1.95 ± 0.02	150 ± 0.6	0.363

Note. The computations were performed for the reference VADM $M_0 = 7.75 \cdot 10^{22}$ A·m^2 and correspond to Figure 3. The shown uncertainties correspond to the 68% confidence interval.

where M is VADM in units of 10^{22} A m^2 and $M_0 = 7.75 \cdot 10^{22}$ A m^2 is the present-day reference VADM. The values of γ for different isotopes are provided in Table 2. While the formula describes the dependence very well, it obviously becomes unstable at $M \rightarrow 0$ and cannot be straightforwardly extrapolated to the period of geomagnetic reversals or excursions when the geomagnetic field cannot be anymore represented by the dominating dipole component (Korte et al., 2019).

Therefore, from the measured production/deposition of cosmogenic isotopes in relation to extreme SEP events or candidates, one can directly and straightforwardly assess (within $\pm 20\%$ for the known VADM) several spectral points of the SEP energy spectrum, without any assumptions of the exact spectral shape.

### 3.4. An Example of Application to the Extreme Solar Events in the Past

As an example of the application of the effective-energy concept for a simple assessment of the SEP events recorded in cosmogenic proxy data, we considered here extreme solar events discovered recently over the last millennia (see s review Miyake et al., 2020). Presently, three confirmed extreme SEP events are known: 774/5 CE originally discovered by Miyake et al. (2012) in Δ^{14}C measured in a Japanese cedar tree and later confirmed in other datasets (Büntgen et al., 2018; Sukhodolov et al., 2017; Usoskin et al., 2013; Uusitalo et al., 2018); 660 BCE discovered by Park et al. (2017) and confirmed later (Büntgen et al., 2018; O'Hare et al., 2019); and 993 CE discovered by Miyake et al. (2013) and confirmed later (Mekhaldi et al., 2015; Sakurai et al., 2020). In addition, three candidates to extreme SEP events have been found recently in ^{14}C datasets and are pending confirmation with other isotopes: 1052 CE and 1279 CE were discovered by Brehm et al. (2021), and 5410 BCE by Miyake et al. (2021).

For all these events we have calculated the fluence $F_{234} \equiv F (>234$ MeV) based on ^{14}C data following the methodology developed here, as shown in Table 3. First, from the published values of the ^{14}C production rates Q and geomagnetic dipole strength VADM M for each event, we computed the production rate Q_{M_0} reduced to the standard geomagnetic conditions using Equation 5. Next, using Equation 2, we calculated the omnidirectional fluence F_{234}, where the values of E_{eff} and $\mathcal{K}_{eff}$ were obtained from Table 2. Finally, the obtained fluence F_{234} was compared with that for the GLE#5 $(1.38 \pm 0.37) \cdot 10^8$ cm^{-2} (Koldobskiy et al., 2021) as the R_{1956} value. The events in Table 3 are sorted by their (corrected for the VADM value) strength. The strongest SEP event of 774 CE was approximately 70 times stronger than the GLE#5 making it an extreme and maximum known event. Other events take the R_{1956} value from 15 to 70 (within uncertainties) reflecting the occurrence probability distribution of the extreme SEP events. It is interesting that three event candidates have the R_{1956} value of 20–30 which approached the theoretical sensitivity limit of the ^{14}C method of $R_{1956} = 15$ (Usoskin et al., 2020).

It should be noted that the R_{1956} values in Table 3 are approximate as based only on ^{14}C data, while other isotopes may lead to slightly different values. A more detailed study will form a subject to a forthcoming work.
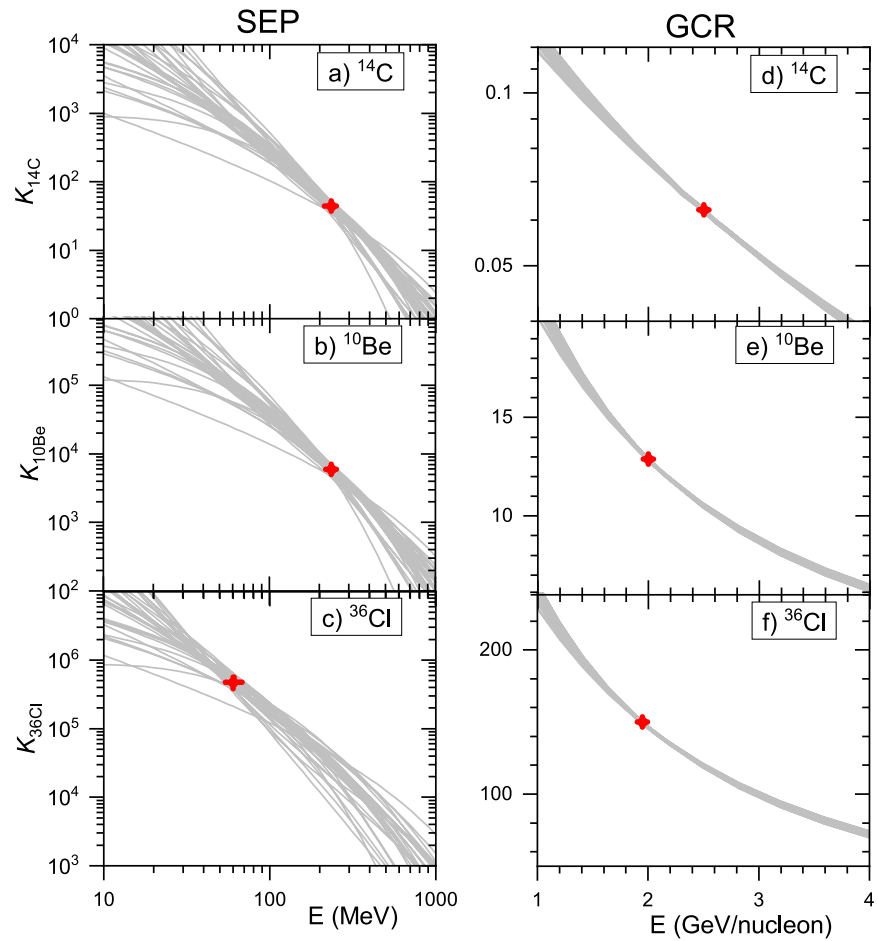
Figure 3. "Bow-tie" plot of the relation between $\mathcal{K}$ and E (Equation 1) for cosmogenic isotopes ^{14}C, ^{10}Be and ^{36}Cl. Left-hand-side (a–c) panels correspond to solar energetic particles (SEPs), where gray curves correspond to different SEP annual fluences (Table 1). Right-hand-side (d–f) panels correspond to galactic cosmic rays (GCRs), where gray curves correspond to GCR nucleonic spectra for different Bartels rotations. The geomagnetic dipole moment (VADM) M is set to $7.75 \cdot 10^{22}$ A m^2. The red dots depict the best-fit values of $\mathcal{K}_{eff}$ and E_{eff} (see Table 2), while red crosses denote the 68% confidence levels.
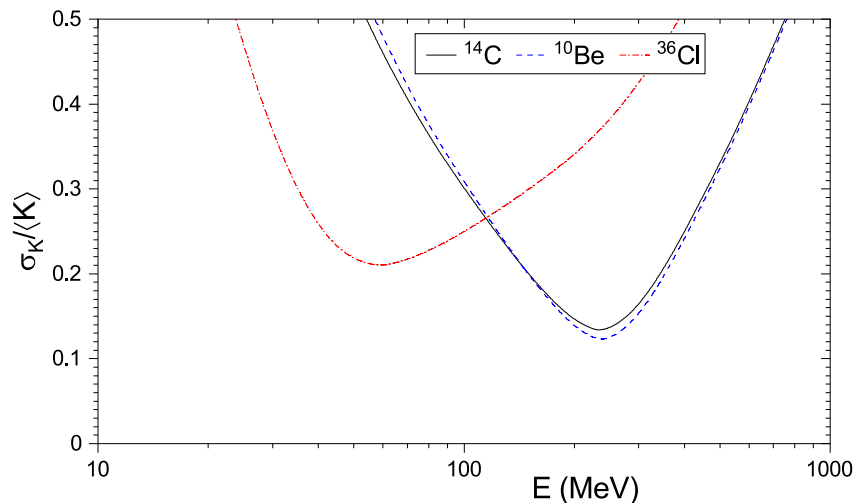
Figure 4. Relative dispersion of the scaling factor, $\sigma_{\mathcal{K}}/\langle \mathcal{K} \rangle$ as function of energy E, for different isotopes (see the text) produced by solar energetic particles.
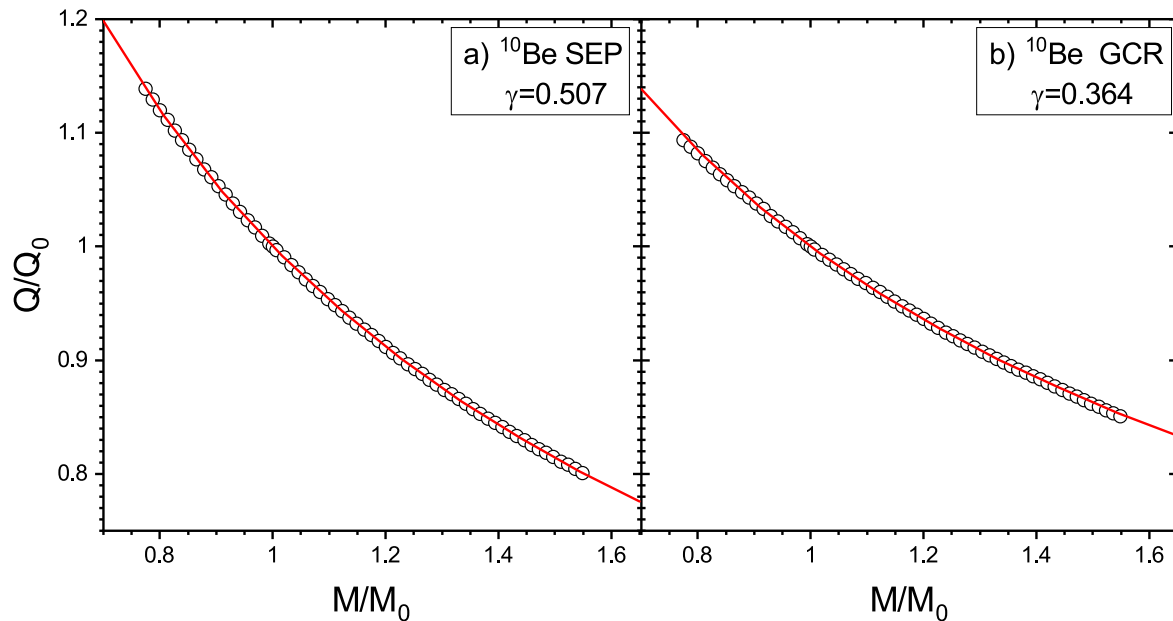
Figure 5. Dependence of the ^{10}Be production/deposition Q, normalized to the production Q_0 at the reference virtual axial dipole moment (VADM) M_0, on the changes of VADM M, as computed for the mean solar energetic particle (panel a) and galactic cosmic ray (panel b) productions. The reference VADM $M_0 = 7.75 \cdot 10^{22}$ A m^2 corresponds to the modern epoch. The red dashed lines denote the dependence (Equation 5) with the best-fit indices γ denoted in the legend.

4. Effective Energy for Galactic Cosmic Rays

In this Section, we computed the effective energy for the production of the three cosmogenic isotopes by GCR. As the spectra of GCR, we considered direct measurements of protons, helium and heavier species performed by the AMS-02 experiment (Aguilar et al., 2017, 2018a, 2018b) during the period of 2011–2017 with a 27-day (Bartels rotations, BRs) cadence. The data set covers 79 BRs from 15-May-2011 (start of BR # 2426) through 09-May-2017 (end of BR # 2506) corresponding to the period from the mid-ascending to the mid-descending phases of solar cycle #24 and characterized by moderate modulation of GCR. By considering directly measured spectra of GCRs, we avoid uncertainties related to the modeled GCR spectra (Asvestari, Gil, et al., 2017; Herbst et al., 2010). In contrast to SEPs consisting mostly of protons, GCR include also helium and heavier species whose contribution to the atmospheric effects can be significant (Koldobskiy, Bindi, et al., 2019). Since heavier species are modulated and shielded by magnetic fields differently with respect to protons of the same energy, they cannot be represented by a simple scaling of protons. Accordingly, we consider the GCR spectrum of not only protons but also heavier species reduced to that of nucleons with the energy expressed per nucleon.

Table 3
Known Extreme Solar Events in ^{14}C Sorted by Their Strength

Event[a]	Q[b]	Reference[c]	M[d]	Q_{M_0}[e]	F_{234}[f]	R_{1956}[g]
774 CE	1.88 ± 0.1	B18	10.3 ± 0.4	2.2 ± 0.1	9.6 ± 0.6	70 ± 19
660 BCE	1.4 ± 0.1	B18	11.4 ± 0.4	1.7 ± 0.1	7.6 ± 0.6	55 ± 15
993 CE	1.04 ± 0.1	S20	10.4 ± 0.4	1.2 ± 0.1	5.4 ± 0.6	39 ± 11
1279 CE	0.77 ± 0.2	B21	10.1 ± 0.2	0.89 ± 0.23	3.9 ± 1	28 ± 10
5410 BCE	0.9 ± 0.1	M21	7.1 ± 0.7	0.86 ± 0.1	3.8 ± 0.5	27 ± 8
1052 CE	0.62 ± 0.12	B21	10.3 ± 0.2	0.72 ± 0.14	3.2 ± 0.6	23 ± 8

[a]The event year. [b]The global ^{14}C production Q (10^8 cm^{-2}) corresponding to the measurements. [c]Reference to the ^{14}C data (Büntgen et al. (2018) - B18, Sakurai et al. (2020) - S20, Miyake et al. (2021) - M21, Brehm et al. (2021) - B21.). [d]VADM M in units of 10^{22} A m^2 as obtained from Usoskin et al. (2016). [e]The production rate reduced to the standard conditions Q_{M_0} in (10^8 cm^{-2}). [f]The omnidirectional fluence $F_{234} \equiv F(>234$ MeV) in (10^9 cm^{-2}), computed here. [g]An approximate ratio of the strength of the SEP event of 23 February 1956 (GLE #5) R_{1956}.

4.1. Differential Response Function

Similarly to SEPs, we computed the differential response function for GCR nucleons as shown in Figure 2 (panels d–f). Panel d depicts the energy spectrum of all nucleons of GCR defined as

$$J_{\mathrm{n}}(E) = \sum_i A_i \cdot J_i(E),$$

(6)

where $J_i(E)$ is the energy spectrum of ith specie of GCR with atomic mass A_i, and E represents kinetic energy per nucleon. Panel e shows the differential response function. One can see that it peaks at much higher energies than that for SEPs reflecting the different spectra of GCR and SEPs. The shape of the response functions for both ^{10}Be and ^{36}Cl produced by spallation reactions are nearly identical to each other, while ^{14}C produced by (n,p) reactions is slightly more sensitive to CR in the energy range of 3–20 GeV. The response functions for all the studied isotopes peak at around 1.5 GeV energy, while the peak of the polar sea-level NM response corresponds to the energy of about 5 GeV.

Figure 2f depicts the cumulative relative contribution, which defines the median energies, that are 4.5, 4.5, 5.9 and 11 GeV for the ^{10}Be, ^{36}Cl, ^{14}C and polar NM, respectively. The median energy for the polar NM is consistent with earlier estimates (Ahluwalia & Fikani, 2007). This is nearly an order of magnitude higher than those for SEPs.

4.2. Effective Energy

The "bow-tie" plots for $\mathcal{K} = J_{\mathrm{n}}(>E)/Q$ for GCR are shown in Figures 3d–3f, where each gray curve corresponds to one BR of AMS-02 data. One can see that the curves lie more compact than for SEP events (Figures 3a–3c) reflecting the fact that variability of GCRs is smaller and more regular than that for SEPs. The effective scaling $\mathcal{K}_{\mathrm{eff}}$ and energy E_{eff} are defined in the same way as for SEPs and listed in the right-hand-side block of Table 2. Since the standard way of quantifying the GCR flux is the intensity in units of $(\mathrm{cm}^2\ \mathrm{sr\ s\ GeV})^{-1}$, the scaling $\mathcal{K}_{\mathrm{eff}}$ has the dimension of sr^{-1} in contrast to SEP fluences where it is dimensionless. The effective energy was found very close to each other for ^{10}Be and ^{36}Cl, being about 2 GeV/nucleon. The effective energy for ^{14}C appeared slightly higher, viz. about 2.5 GeV/nucleon. This is related to the fact that ^{14}C is produced globally, while ^{10}Be and ^{36}Cl are more weighted, because of the atmospheric transport/deposition pattern, toward higher latitudes with lower geomagnetic cutoffs.

4.3. Dependence on the Geomagnetic Field

The dependence of the isotope's production rate by GCR on the geomagnetic field strength, quantified via the VADM M is shown in Figure 5b for ^{10}Be produced by GCR. It can be seen that the computed dependence is nearly perfectly described by formula 5 with the index $\gamma = 0.364$ (see Table 2). Similar dependencies for other isotopes (not shown) are equally well described by formula 5 with indices listed in Table 2. The dependence is stronger ($\gamma = 0.546$) for the globally produced ^{14}C than for mid/high-latitude dominated production and transport of ^{10}Be and ^{36}Cl.

4.4. An Example of GCR Intensity Variability Over the Last Millennium

As an example of the application of the effective energy approach to GCR, we show in Figure 6 estimate of the integral intensity J (>2.48 GeV/nuc) of GCR over the last millennium, since 970 CE. The estimate is based on the recent reconstruction of the annual ^{14}C global production rate by Brehm et al. (2021) for the last millennium. Conversion to the standard geomagnetic conditions $M_0 = 7.75 \cdot 10^{22}$ A m^2 was made by a Monte-Carlo approach (similar to Usoskin et al., 2021) by randomly selecting values of M for each year from four alternative archeomagnetic reconstructions (Hellio & Gillet, 2018; Nilsson et al., 2014; Pavón-Carrasco et al., 2014; Usoskin et al., 2016) and applying the correction using formula 5. Then the corrected production rate was converted, using Equation 1 with values E_{eff} and $\mathcal{K}_{\mathrm{eff}}$ from Table 2, into the integral flux of GCR nucleons J (>2.48 GeV), which is shown by the solid black line. The uncertainties (gray shaded area) were assessed by the Monte-Carlo method (see methodology in Usoskin et al., 2021) considering those of ^{14}C measurements, geomagnetic field strength M and the coefficient $\mathcal{K}_{\mathrm{eff}}$. One can see that the flux varies at different time scales: there is a clear 11-year cycle
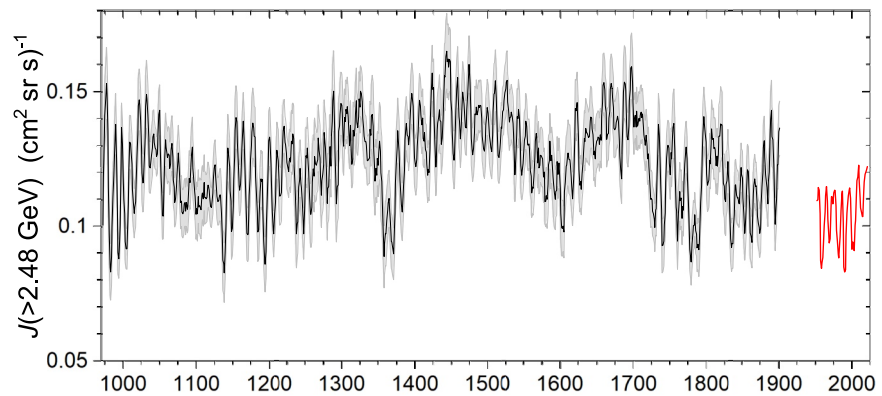
Figure 6. Time profile of the galactic cosmic ray integral nucleonic flux J (>2.48 GeV/nuc), estimated using the ^{14}C annual production rate for the last millennium (Brehm et al., 2021; Usoskin et al., 2021). The 68% confidence level uncertainties are shown by the gray shaded area. The red line depicts the annual values of F (>2.48 GeV/nuc) calculated from the NM network data since 1951.

and a secular variability caused by the changing solar-activity level (Usoskin, 2017), including grand solar minima ca 1050 (Oort minimum), 1300 (Wolf), 1400 (Spörer), 1700 (Maunder) and 1800 (Dalton). Because of the anthropogenic Suess effect (extensive use of fossil fuel which dilutes ^{14}C in the atmosphere – Suess, 1955) and bomb-effect (nuclear tests produce a large amount of ^{14}C), radiocarbon can be hardly used as a cosmic-ray index after the onset of the industrial revolution.

For comparison, we also show, as the red curve in Figure 6, the J (>2.48 GeV/nuc) flux directly computed since 1951 from the world NM-network data using the methodology of Usoskin et al. (2017) and Koldobskiy, Bindi, et al. (2019). It can be seen that the level of GCR is significantly lower in the second half of the twentieth century than that for the millennium before. It is comparable only to a short period ca. 1350 CE between Wolf and Spörer grand minima. This systematically reduced flux of GCR corresponds to the Modern grand maximum of solar activity (Usoskin, 2017). On the other hand, the GCR flux was higher during the last two weaker solar cycles being comparable to that of the late nineteenth century, in agreement with the solar activity estimates (e.g., Hathaway, 2015). This indirectly confirms the validity of our approach and the overall agreement between indirect ^{14}C-based method to estimate cosmic-ray variability and direct estimates for the modern era.

5. Conclusions

Here we developed and proposed a simple and quick "effective energy" method to estimate the flux of cosmic-ray particles directly from concentrations of cosmogenic isotopes ^{14}C, ^{10}Be and ^{36}Cl measured in natural archives. Even though the method is simple, it is based on full detailed simulations of the production and transport of the cosmogenic isotopes in the terrestrial environment, including the thoroughly computed effective yield function tabulated in the Supporting Information S1.

The method is based on an assumption that there is such effective energy E_{eff} that the relation between the flux of CR particles with energy above it F (>E_{eff}) is directly proportional to the measured concentration of the isotope (Equation 3), irrespectively of the exact energy spectrum of CR particles. We first verified this assumption separately for SEPs and GCRs (Figure 3) using the data of recorded GLE events for the last 60 years for SEPs and the space-borne measurements by AMS-02 detector from 2011 to 2017 for GCR. We calculated the values of the effective energy E_{eff} and the scaling factor $\mathcal{K}_{\text{eff}}$ separately for each isotope and each type of CRs, as presented in Table 2. The accuracy of the method is within 20% for SEP and within 1% for GCR. To account for the variable geomagnetic field quantified through the VADM concept, we provided a simple way (Equation 5) to reduce the measured data to the standard conditions corresponding to the modern epoch with VADM $M_0 = 7.75 \cdot 10^{22}$ A m^2.

As an illustration, the method was applied to the data of ^{14}C for six known extreme SEP events or candidates that allowed us to rank these events by strength in comparison to the strongest directly observed SEP event of 23-Feb-1956 (GLE#5), as summarized in Table 3. We also provided, as an example, the temporal evolution of the integral nucleonic flux of GCR J (>2.48 GeV/nuc) over the last millennium (Figure 6) as based on the recent data of the

annual ^{14}C global production rates. The estimated flux agrees well with that calculated from the direct NM data for the last decades, providing an indirect verification of the method.

Thus, we have developed an approximate method for a simple and quick estimate of the CR integral fluxes directly from the measured cosmogenic isotope measurements (production rate or depositional flux) for SEPs and GCRs. This makes a useful tool for rough assessments of the CR variability and spectra. However, the proposed method does not supersede the full modeling of the isotope production and transport that is still required for precise data analysis and interpretation.

Data Availability Statement

Spectra of solar energetic particles can be computed from the information presented by Koldobskiy et al. (2021), viz. parameters (Table 2) therein applied to Equations 1–3 therein. Spectra of GCR are available from AMS-02 data (Aguilar et al., 2018a), collected in the Cosmic Ray Database https://tools.ssdc.asi.it/CosmicRays (Di Felice et al., 2017).

References

Aguilar, M., Ali Cavasonza, L., Alpat, B., Ambrosi, G., Arruda, L., Attig, N., & Zuccon, P. (2017). Observation of the identical rigidity dependence of He, C, and O cosmic rays at high rigidities by the alpha magnetic spectrometer on the international space station. *Physical Review Letters*, *119*, 251101. https://doi.org/10.1103/PhysRevLett.119.251101

Aguilar, M., Ali Cavasonza, L., Alpat, B., Ambrosi, G., Arruda, L., Attig, N., & Zuccon, P. (2018a). Observation of fine time structures in the cosmic proton and helium fluxes with the alpha magnetic spectrometer on the international space station. *Physical Review Letters*, *121*(5), 051101. https://doi.org/10.1103/PhysRevLett.121.051101

Aguilar, M., Ali Cavasonza, L., Alpat, B., Ambrosi, G., Arruda, L., Attig, N., & Zuccon, P. (2018b). Precision measurement of cosmic-ray nitrogen and its primary and secondary components with the alpha magnetic spectrometer on the international space station. *Physical Review Letters*, *121*, 051103. https://doi.org/10.1103/PhysRevLett.121.051103

Ahluwalia, H. S., & Fikani, M. M. (2007). Cosmic ray detector response to transient solar modulation: Forbush decreases. *Journal of Geophysical Research*, *112*, A08105. https://doi.org/10.1029/2006JA011958

Alanko, K., Usoskin, I. G., Mursula, K., & Kovaltsov, G. A. (2003). Heliospheric modulation strength: Effective neutron monitor energy. *Advances in Space Research*, *32*, 615–620. https://doi.org/10.1016/S0273-1177(03)00348-X

Asvestari, E., Gil, A., Kovaltsov, G. A., & Usoskin, I. G. (2017). Neutron monitors and cosmogenic isotopes as cosmic ray energy-integration detectors: Effective yield functions, effective energy, and its dependence on the local interstellar spectrum. *Journal of Geophysical Research: Space Physics*, *122*, 9790–9802. https://doi.org/10.1002/2017JA024469

Asvestari, E., Willamo, T., Gil, A., Usoskin, I., Kovaltsov, G., Mikhailov, V., & Mayorov, A. (2017). Analysis of ground level enhancements (GLE): Extreme solar energetic particle events have hard spectra. *Advances in Space Research*, *60*, 781–787. https://doi.org/10.1016/j.asr.2016.08.043

Beer, J. (2000). Neutron monitor records in broader historical context. *Space Science Reviews*, *93*, 107–119. https://doi.org/10.1023/A:1026536226656

Beer, J., McCracken, K., & von Steiger, R. (2012). *Cosmogenic radionuclides: Theory and applications in the terrestrial and space environments*. Springer.

Brehm, N., Bayliss, A., Christl, M., Synal, H., Adolphi, F., Beer, J., & Wacker, L. (2021). Eleven-year solar cycles over the last millennium revealed by radiocarbon in tree rings. *Nature Geoscience*, *14*, 10–15. https://doi.org/10.1038/s41561-020-00674-0

Büntgen, U., Wacker, L., Galvan, J., Arnold, S., Arseneault, D., Baillie, M., & Young, G. H. F. (2018). Tree rings reveal globally coherent signature of cosmogenic radiocarbon events in 774 and 993 CE. *Nature Communications*, *9*, 3605. https://doi.org/10.1038/s41467-018-06036-0

Cliver, E. W., Mekhaldi, F., & Muscheler, R. (2020). Solar longitude distribution of high-energy proton flares: Fluences and spectra. *The Astrophysical Journal Letters*, *900*(1), L11. https://doi.org/10.3847/2041-8213/abad44

Desai, M., & Giacalone, J. (2016). Large gradual solar energetic particle events. *Living Reviews in Solar Physics*, *13*, 3. https://doi.org/10.1007/s41116-016-0002-5

Di Felice, V., Pizzolotto, C., D'Urso, D., Dari, S., Navarra, D., Primavera, R., & Bertucci, B. (2017). Looking for cosmic ray data? The ASI cosmic ray database. In *Proceedings of the 35th international cosmic ray conference (ICRC2017), Busan, Korea* (pp. 10–20).

Hathaway, D. H. (2015). The solar cycle. *Living Reviews in Solar Physics*, *12*, 4. https://doi.org/10.1007/lrsp-2015-4

Heikkilä, U., Beer, J., Abreu, J. A., & Steinhilber, F. (2013). On the atmospheric transport and deposition of the cosmogenic radionuclides (^{10}Be): A review. *Space Science Reviews*, *176*, 321–332. https://doi.org/10.1007/s11214-011-9838-0

Heikkilä, U., Beer, J., & Feichter, J. (2009). Meridional transport and deposition of atmospheric ^{10}Be. *Atmospheric Chemistry and Physics*, *9*, 515–527. https://doi.org/10.5194/acp-9-515-2009

Hellio, G., & Gillet, N. (2018). Time-correlation-based regression of the geomagnetic field from archeological and sediment records. *Geophysical Journal International*, *214*(3), 1585–1607. https://doi.org/10.1093/gji/ggy214

Herbst, K., Kopp, A., Heber, B., Steinhilber, F., Fichtner, H., Scherer, K., & Matthiä, D. (2010). On the importance of the local interstellar spectrum for the solar modulation parameter. *Journal of Geophysical Research*, *115*, D00I20. https://doi.org/10.1029/2009JD012557

Jull, A., Panyushkina, I., Lange, T., Kukarskih, V., Myglan, V., Clark, K., & Leavitt, S. (2014). Excursions in the ^{14}C record at AD 774–775 in tree rings from Russia and America. *Geophysical Research Letters*, *41*, 3004–3010. https://doi.org/10.1002/2014GL059874

Koldobskiy, S. A., Bindi, V., Corti, C., Kovaltsov, G., & Usoskin, I. (2019). Validation of the neutron monitor yield function using data from AMS-02 experiment 2011–2017. *Journal of Geophysical Research: Space Physics*, *124*, 2367–2379. https://doi.org/10.1029/2018JA026340

Koldobskiy, S. A., Kovaltsov, G. A., Mishev, A. L., & Usoskin, I. G. (2019). New method of assessment of the integral fluence of solar energetic (>1 GV rigidity) particles from neutron monitor data. *Solar Physics*, *294*(7), 94. https://doi.org/10.1007/s11207-019-1485-8

Koldobskiy, S. A., Raukunen, O., Vainio, R., Kovaltsov, G., & Usoskin, I. (2021). New reconstruction of event-integrated spectra (spectral fluences) for major solar energetic particle events. *Astronomy and Astrophysics*, *647*, A132. https://doi.org/10.1051/0004-6361/202040058

Korte, M., Brown, M. C., Panovska, S., & Wardinski, I. (2019). Robust characteristics of the Laschamp and mono lake geomagnetic excursions: Results from global field models. *Frontiers of Earth Science*, *7*, 86. https://doi.org/10.3389/feart.2019.00086

Korte, M., & Constable, C. (2005). The geomagnetic dipole moment over the last 7000 years—New results from a global model. *Earth and Planetary Science Letters*, *236*, 348–358. https://doi.org/10.1016/j.epsl.2004.12.031

Korte, M., Constable, C., Donadini, F., & Holme, R. (2011). Reconstructing the Holocene geomagnetic field. *Earth and Planetary Science Letters*, *312*, 497–505. https://doi.org/10.1016/j.epsl.2011.10.031

Kovaltsov, G. A., Usoskin, I. G., Cliver, E. W., Dietrich, W. F., & Tylka, A. J. (2014). Fluence ordering of solar energetic proton events using cosmogenic radionuclide data. *Solar Physics*, *289*, 4691–4700. https://doi.org/10.1007/s11207-014-0606-7

Mekhaldi, F., Adolphi, F., Herbst, K., & Muscheler, R. (2021). The signal of solar storms embedded in cosmogenic radionuclides: Detectability and uncertainties. *Journal of Geophysical Research*, *126*, e2021JA029351. https://doi.org/10.1029/2021JA029351

Mekhaldi, F., Muscheler, R., Adolphi, F., Aldahan, A., Beer, J., McConnell, J., & Woodruff, T. (2015). Multiradionuclide evidence for the solar origin of the cosmic-ray events of AD 774/5 and 993/4. *Nature Communications*, *6*, 8611. https://doi.org/10.1038/ncomms9611

Mishev, A., Koldobskiy, S., Kovaltsov, G., Gil, A., & Usoskin, I. (2020). Updated neutron-monitor yield function: Bridging between in-situ and ground-based cosmic ray measurements. *Journal of Geophysical Research: Space Physics*, *125*, e2019JA027433. https://doi.org/10.1029/2019JA027433

Miyake, F., Masuda, K., & Nakamura, T. (2013). Another rapid event in the carbon-14 content of tree rings. *Nature Communications*, *4*, 1748. https://doi.org/10.1038/ncomms2783

Miyake, F., Nagaya, K., Masuda, K., & Nakamura, T. (2012). A signature of cosmic-ray increase in AD 774–775 from tree rings in Japan. *Nature*, *486*, 240–242. https://doi.org/10.1038/nature11123

Miyake, F., Panyushkina, I. P., Jull, A. J. T., Adolphi, F., Brehm, N., Helama, S., & Wacker, L. (2021). A single year cosmic ray event at 5410 BCE registered in ^{14}C of tree rings. *Geophysical Research Letters*, *48*, e2021GL093419. https://doi.org/10.1029/2021GL093419

Miyake, F., Usoskin, I., & Poluianov, S. (Eds.), (2020). *Extreme solar particle storms: The hostile sun*. IOP Publishing. https://doi.org/10.1088/2514-3433/ab404a

Nilsson, A., Holme, R., Korte, M., Suttie, N., & Hill, M. (2014). Reconstructing Holocene geomagnetic field variation: New methods, models and implications. *Geophysical Journal International*, *198*, 229–248. https://doi.org/10.1093/gji/ggu120

O'Hare, P., Mekhaldi, F., Adolphi, F., Raisbeck, G., Aldahan, A., Anderberg, E., & Muscheler, R. (2019). Multiradionuclide evidence for an extreme solar proton event around 2,610 B.P. (660 BC). *Proceedings of the National Academy of Sciences*, *116*(13), 5961–5966. https://doi.org/10.1073/pnas.1815725116

Park, J., Southon, J., Fahrni, S., Creasman, P. P., & Mewaldt, R. (2017). Relationship between solar activity and ^{14}C peaks in AD 775, AD 994, and 660 BC. *Radiocarbon*, *59*, 1147–1156. https://doi.org/10.1017/rdc.2017.59

Pavón-Carrasco, F. J., Osete, M. L., Torta, J. M., & De Santis, A. (2014). A geomagnetic field model for the Holocene based on archeomagnetic and lava flow data. *Earth and Planetary Science Letters*, *388*, 98–109. https://doi.org/10.1016/j.epsl.2013.11.046

Poluianov, S., Kovaltsov, G. A., Mishev, A. L., & Usoskin, I. G. (2016). Production of cosmogenic isotopes ^{7}Be, ^{10}Be, ^{14}C, ^{22}Na, and ^{36}Cl in the atmosphere: Altitudinal profiles of yield functions. *Journal of Geophysical Research*, *121*, 8125–8136. https://doi.org/10.1002/2016JD025034

Poluianov, S., Kovaltsov, G. A., & Usoskin, I. G. (2018). Solar energetic particles and galactic cosmic rays over millions of years as inferred from data on cosmogenic ^{26}Al in lunar samples. *Astronomy and Astrophysics*, *618*, A96. https://doi.org/10.1051/0004-6361/201833561

Poluianov, S., Usoskin, I., Mishev, A., Shea, M., & Smart, D. (2017). GLE and sub-GLE redefinition in the light of high-altitude polar neutron monitors. *Solar Physics*, *292*, 176. https://doi.org/10.1007/s11207-017-1202-4

Raukunen, O., Paassilta, M., Vainio, R., Rodriguez, J., Eronen, T., Crosby, N., & Sandberg, I. (2020). Very high energy proton peak flux model. *Journal of Space Weather and Space Climate*, *10*, 24. https://doi.org/10.1051/swsc/2020024

Sakurai, H., Tokanai, F., Miyake, F., Horiuchi, K., Masuda, K., Miyahara, H., & Moriya, T. (2020). Prolonged production of ^{14}C during the 660 BCE solar proton event from Japanese tree rings. *Scientific Reports*, *10*, 660. https://doi.org/10.1038/s41598-019-57273-2

Shea, M., & Smart, D. (1990). A summary of major solar proton events. *Solar Physics*, *127*, 297–320. https://doi.org/10.1007/bf00152170

Simpson, J. A. (2000). The cosmic ray nucleonic component: The invention and scientific uses of the neutron monitor. *Space Science Reviews*, *93*, 11–32. https://doi.org/10.1023/A:1026567706183

Suess, H. (1955). Radiocarbon concentration in modern wood. *Science*, *122*, 415–417. https://doi.org/10.1126/science.122.3166.415.b

Sukhodolov, T., Usoskin, I., Rozanov, E., Asvestari, E., Ball, W., Curran, M., & Traversi, R. (2017). Atmospheric impacts of the strongest known solar particle storm of 775 AD. *Scientific Reports*, *7*, 45257. https://doi.org/10.1038/srep45257

Thébault, E., Finlay, C. C., Beggan, C. D., Alken, P., Aubert, J., Barrois, O., & Zvereva, T. (2015). International geomagnetic reference field: The 12th generation. *Earth Planets and Space*, *67*, 79. https://doi.org/10.1186/s40623-015-0228-9

Usoskin, I. G. (2017). A history of solar activity over millennia. *Living Reviews in Solar Physics*, *14*, 3. https://doi.org/10.1007/s41116-017-0006-9

Usoskin, I. G., Gallet, Y., Lopes, F., Kovaltsov, G. A., & Hulot, G. (2016). Solar activity during the Holocene: The Hallstatt cycle and its consequence for grand minima and maxim. *Astronomy and Astrophysics*, *587*, A150. https://doi.org/10.1051/0004-6361/201527295

Usoskin, I. G., Gil, A., Kovaltsov, G. A., Mishev, A. L., & Mikhailov, V. V. (2017). Heliospheric modulation of cosmic rays during the neutron monitor era: Calibration using PAMELA data for 2006–2010. *Journal of Geophysical Research: Space Physics*, *122*, 3875–3887. https://doi.org/10.1002/2016JA023819

Usoskin, I. G., Koldobskiy, S. A., Kovaltsov, G. A., Rozanov, E. V., Sukhodolov, T. V., Mishev, A. L., & Mironova, I. A. (2020). Revisited reference solar proton event of 23 February 1956: Assessment of the cosmogenic-isotope method sensitivity to extreme solar events. *Journal of Geophysical Research*, *125*(6), e27921. https://doi.org/10.1029/2020JA027921

Usoskin, I. G., Kromer, B., Ludlow, F., Beer, J., Friedrich, M., Kovaltsov, G. A., & Wacker, L. (2013). The AD775 cosmic event revisited: The sun is to blame. *Astronomy and Astrophysics*, *552*, L3. https://doi.org/10.1051/0004-6361/201321080

Usoskin, I. G., Solanki, S. K., Krivova, N., Hofer, B., Kovaltsov, G. A., Wacker, L., & Kromer, B. (2021). Solar cyclic activity over the last millennium reconstructed from annual ^{14}C data. *Astronomy and Astrophysics*, *649*, A141. https://doi.org/10.1051/0004-6361/202140711

Uusitalo, J., Arppe, L., Hackman, T., Helama, S., Kovaltsov, G., Mielikäinen, K., & Oinonen, M. (2018). Solar superstorm of AD 774 recorded subannually by Arctic tree rings. *Nature Communications*, *9*, 3495. https://doi.org/10.1038/s41467-018-05883-1

Vainio, R., Desorgher, L., Heynderickx, D., Storini, M., Flückiger, E., Horne, R. B., & Usoskin, I. G. (2009). Dynamics of the Earth's particle radiation environment. *Space Science Reviews*, *147*, 187–231. https://doi.org/10.1007/s11214-009-9496-7

Webber, W., Higbie, P., & McCracken, K. (2007). Production of the cosmogenic isotopes ^{3}H, ^{7}Be, ^{10}Be, and ^{36}Cl in the Earth's atmosphere by solar and galactic cosmic rays. *Journal of Geophysical Research*, *112*, A10106. https://doi.org/10.1029/2007JA012499

Wu, C. J., Usoskin, I. G., Krivova, N., Kovaltsov, G. A., Baroni, M., Bard, E., & Solanki, S. K. (2018). Solar activity over nine millennia: A consistent multi-proxy reconstruction. *Astronomy and Astrophysics*, *615*, A93. https://doi.org/10.1051/0004-6361/201731892